The Astrophysical Journal, 767:121 (6pp), 2013 April 20 doi:10.1088/0004-637X/767/2/121

DISCOVERY OF Fe Kα X-RAY REVERBERATION AROUND THE BLACK HOLES IN MCG–5-23-16 AND NGC 7314

A. Zoghbi[1,2], C. Reynolds[1,2], E. M. Cackett[3], G. Miniutti[4], E. Kara[5], and A. C. Fabian[5]
[1] Department of Astronomy, University of Maryland, College Park, MD 20742-2421, USA; azoghbi@astro.umd.edu
[2] Joint Space-Science Institute (JSI), College Park, MD 20742-2421, USA
[3] Department of Physics & Astronomy, Wayne State University, 666 W. Hancock St, Detroit, MI 48201, USA
[4] Centro de Astrobiologia (CSIC-INTA), Dep. de Astrosica, P.O. Box 78, E-28691 Villanueva de la Cãnada, Madrid, Spain
[5] Institute of Astronomy, Madingley Road, Cambridge CB3 0HA, UK
Received 2012 December 19; accepted 2013 February 7; published 2013 April 4

ABSTRACT

Several X-ray observations have recently revealed the presence of reverberation time delays between spectral components in active galactic nuclei. Most of the observed lags are between the power-law Comptonization component, seen directly, and the soft excess produced by reflection in the vicinity of the black hole. NGC 4151 was the first object to show these lags in the iron *K* band. Here, we report the discovery of reverberation lags in the Fe *K* band in two other sources: MCG–5-23-16 and NGC 7314. In both objects, the 6–7 keV band, where the Fe Kα line peaks, lags the bands at lower and higher energies with a time delay of $\sim$1 ks. These lags are unlikely to be due to the narrow Fe Kα line. They are fully consistent with reverberation of the relativistically broadened iron Kα line. The measured lags, their time scale, and spectral modeling indicate that most of the radiation is emitted at $\sim$5 and 24 gravitational radii for MCG–5-23-16 and NGC 7314, respectively.

Key words: accretion, accretion disks – black hole physics – galaxies: active – galaxies: groups: individual (MCG–5-23-16, NGC 7314) – galaxies: nuclei – gravitation – X-rays: galaxies

Online-only material: color figures

1. INTRODUCTION

Observations of active galactic nuclei (AGN) have shown that most of the X-ray radiation is emitted very close to the central supermassive black hole. Short timescale variability (e.g., Vaughan et al. 2011), relativistic spectral distortions (Tanaka et al. 1995; Reynolds & Nowak 2003; Miller 2007; Fabian et al. 2012b), X-ray eclipses (Risaliti et al. 2007), as well as gravitational micro-lensing measurements (Chartas et al. 2012) all indicate that emission originates in a compact region a few gravitational radii from the event horizon.

The primary X-ray radiation is thought to be produced in a hot electron corona by Compton up-scattering lower energy disk photons (Haardt & Maraschi 1991). This radiation illuminates the surrounding, relatively cold matter (Guilbert & Rees 1988; Fabian et al. 1989) giving rise to characteristic reflection spectra (Ross & Fabian 1993). The variability of the primary X-ray source in this environment naturally leads to time delays comparable to the light-crossing time to the reflector (Reynolds et al. 1999). The first direct evidence for such delays was measured in the narrow-line Seyfert 1 (NLS1) galaxy 1H0707−495 (Fabian et al. 2009; Zoghbi et al. 2010). It was observed as a $\sim$30 s delay between the primary X-ray source and the strong iron L line produced by reflection. Several subsequent studies have shown that such lags are present in many other Seyfert galaxies possessing a soft excess (Emmanoulopoulos et al. 2011; de Marco et al. 2011; Zoghbi & Fabian 2011; Kara et al. 2013a; Fabian et al. 2012a; Cackett et al. 2013). All these delays are comparable to the light-crossing time at a few gravitational radii (r_g) from the black hole, and there is even evidence that the amplitude and frequency of the lag correlates with the black hole mass (De Marco et al. 2013).

A key property in all those objects is their strong soft excess, a characteristic feature in the NLS1 class. The measured time delays between the direct power-law component, which dominates the 2–4 keV band, and the soft excess (<1 keV) are naturally explained if the latter is due to a reflection process. In this case, a combination of emission lines and bremsstrahlung from the surface layers of an ionized disk are smoothed and distorted by relativistic effects. Interpreting the measured lags as light-crossing effects in the immediate vicinity of the black hole was questioned by Miller et al. (2010) who argued that these delays could be an artifact of a much larger system (hundreds of r_g). Although such an interpretation fails when a full set of observed timing and spectroscopic properties are considered (Zoghbi et al. 2011), it partly stands on the ambiguity of interpreting the soft excess itself. The spectrum of the observed soft excess tends to be very smooth masking out any direct detection of spectral emission features. Detecting lags in the iron K part of the spectrum ($\sim$6 keV) removes such ambiguity.

More recently, for the first time time lags have been measured in NGC 4151 in the iron *K* band (Zoghbi et al. 2012). Using archival *XMM-Newton* observations, a time delay of a few kiloseconds was measured between the 2–3 keV band of the direct emission and the peak of the Fe Kα line. The change of lag with energy resembles the shape of an iron Kα line broadened by relativistic effects. In addition, the "line" has a stronger blue horn at long timescales and a prominent red wing at short timescales, in a striking match to the expectation of a line emitted from a disk and distorted by relativistic effects (Fabian et al. 1989). Detection of Fe K lags has also been seen in 1H0707−495 (Kara et al. 2013a) and IRAS 13224−3809 (Kara et al. 2013a). Here, we report on the detection of similar lags in two Seyfert galaxies MCG–5-23-16 and NGC 7314 using *XMM-Newton* observations. The two objects were selected because of their brightness and high variability in the 2–10 keV band. Their selection came during the search for the best reverberation targets for the proposed X-ray mission GRAVITAS (Nandra et al. 2012).

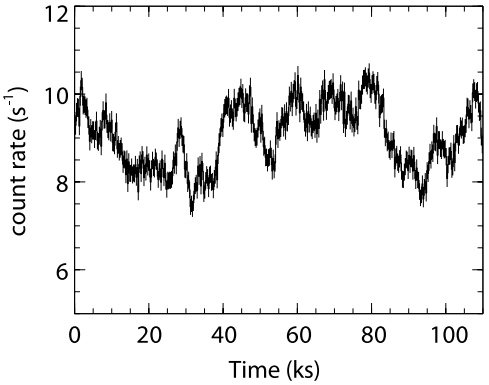

Figure 1. Light curve of MCG–5-23-16 in the 2–10 energy band. It shows the high count rate and strong variability.

MCG–5-23-16 is a Seyfert 1.9 Galaxy ($z = 0.0085$) with a typical 2–10 keV flux of $\sim 8 \times 10^{-11}$ erg cm^{-2} s^{-1} and a mass of $5 \times 10^7 M_\odot$ (Wandel & Mushotzky 1986). Its spectrum resembles a classical Compton-thin Seyfert 2 galaxy with a column that does not affect the spectrum above 3 keV significantly. The spectrum below 1 keV contains a combination of emission from scattered continuum photons and distant photoionized gas. Above 2 keV, the spectrum shows both the narrow (EW $\sim$ 60 eV) and broad (EW $\sim$ 50–200 eV) iron Kα lines along with a strong Compton hump above 10 keV (Weaver et al. 1997; Mattson & Weaver 2004; Braito et al. 2006; Reeves et al. 2007).

NGC 7314 is also classified as a Seyfert 1.9 galaxy ($z = 0.0048$) with an estimated mass of 5×10^6 $M_\odot$ (Schulz et al. 1994). It shows strong variability on all observed timescales. It is thought to be a type-2 counterpart to the NLS1 class (Dewangan & Griffiths 2005). The source is possibly seen through a weak warm absorber. The iron *K* band also shows both the narrow and broad components in observations with *ASCA*, *Chandra*, and *XMM* (Yaqoob et al. 1996, 2003; Ebrero et al. 2011). It has also been shown that the narrow and broad components of the line respond differently to variations in the continuum (Yaqoob et al. 2003). Both objects show hard and absorbed spectra. We concentrate in our analysis on energies >2 keV to avoid any spectral complexities due to either emission from scattered and distant continuum photons and photoionized gas, or from warm absorption.

The paper is organized as follows. Section 2 describes the data used in the analysis. The results for MCG–5-23-16 and NGC 7314 are presented in Sections 3 and 4, respectively, which include both lag and spectral modeling. The interpretation and implications of the results are presented in Section 5.

2. DATA ANALYSIS

The results presented here are obtained using archival *XMM* observations of MCG–5-23-16 and NGC 7314. MCG–5-23-16 was observed three times (ObsIDs: 0112830301, 0112830401, and 0302850201). The first had a strong particle background and was not used. The second observation was short (20 ks after high background filtering) and not very useful for timing analysis. Only the third long observation was used for timing (exposure 130 ks) after removing the last $\sim$20 ks affected by strong particle background in the detector. This observation was taken in the large-window mode and had some pileup, with a deviation from the model by 1.6% and 3.7% for the single and double patterns, respectively (as measured by `epatplot` in SAS). Pileup is not an issue for timing analysis as shown by

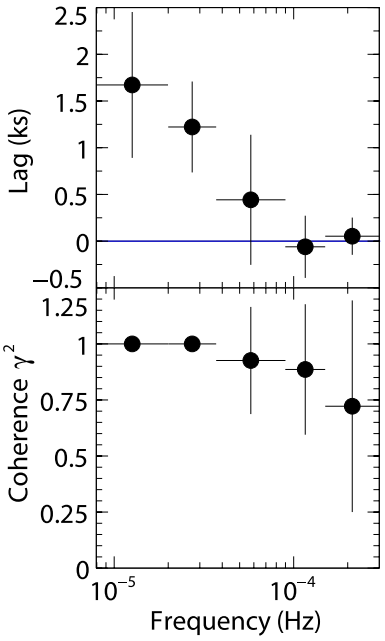

Figure 2. Lag (top) and coherence (bottom) as a function of Fourier frequency between the 4–5 and 6–7 keV energy bands for MCG–5-23-16. Positive lags in the top panel indicate hard lags, where the harder band (6–7 keV, where the reflected iron K line peaks) lags the softer band (4–5 keV, dominated by the direct emission). There is a significant hard lag at frequencies $<10^{-4}$ Hz. The measured coherence remains high at those frequencies.

(A color version of this figure is available in the online journal.)

Zoghbi & Fabian (2011), who performed detailed simulations on the effect of pileup on lag measurements. The central regions were exercised in the spectral modeling to remove the most affected regions in the Point Spread Function (PSF). NGC 7314 was observed only once (ObsID: 0111790101; exposure 44 ks) in a small-window mode with an additional one off-axis observation (ObsID: 0311190101; exposure 83 ks) and both observations were used. The Observation Data Files were reduced with the standard pipeline using SAS 12.0.1. Source and background light curves were extracted from circular regions of 50 arcsec radii from the pn detector. The light curves were then corrected for instrumental effects using `epiclccorr`. Spectra and responses were extracted following the standard procedure in the *XMM* ABC guide.

3. MCG–5-23-16

3.1. Time Lags

Figure 1 shows the 2–10 keV light curve. The object is clearly very bright and variable. To study time lags, light curves were constructed in eight energy bins between 2 and 10 keV with 1 keV bin width. We used standard Fourier techniques to calculate the frequency-dependent time lags (Nowak et al. 1999) and found that the lag depends on both the frequency and energy bands used. As an example, Figure 2 (top) shows the frequency-dependent lag between the 4–5 and 6–7 keV energy bands. We use the standard sign convention, where positive values indicate a hard lag (i.e., the harder band is delayed with respect to the softer band). It is clear that the 6–7 keV band lags behind the 4–5 keV band below 10^{-4} Hz. The bottom panel of Figure 2 shows the measured coherence function γ^2 (Vaughan & Nowak 1997). This is a measure of the fraction of one light curve that can be predicted from the other. It can be seen that the coherence is high and the light curves match each other's variability.

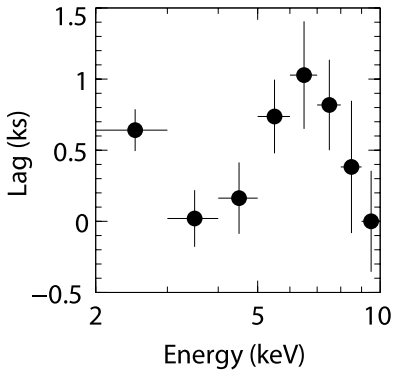

Figure 3. Lag as a function of energy for frequencies $<10^{-4}$ for MCG–5-23-16. Energy bins have a width of 1 keV. The lags are measured with respect to a reference band taken to be the whole 2–10 keV band (see the text for details).

In order to study the energy dependence of the lag, we select the frequency band where there is a positive lag in Figure 2 (top), i.e., $f < 10^{-4}$ Hz, and calculate the lag for the different energy bands with respect to a reference band. The reference can be any band, or can be the total 2–10 keV band itself. Here, for each energy band, the reference band is taken to be the whole 2–10 keV band excluding the current band. Using the whole band as a reference maximizes the signal to noise, while removing the band of interest from the reference ensures that the noise remains uncorrelated (see Zoghbi et al. 2011). The result is a plot of the lag at frequencies $<0^{-4}$ Hz as a function of energy, and it is shown in Figure 3.

Figure 3 clearly shows that the lag traces the shape of a line that peaks in the 6–7 keV band, where the iron Kα line peaks. This is similar to the shape reported for NGC 4151 (Zoghbi et al. 2012), but appears to be less broad. Note that the zero point in Figure 3 (and the rest of the lag–energy plots in this work) depends on the chosen reference band, but for clarity we have shifted the plot vertically so that the zero point is the point with the most negative lag (the last point in this case). Note also that the average value of the positive lag at frequencies $<10^{-4}$ Hz in Figure 2 (top) is $\sim$0.7 ks, which is the value of the vertical difference between the 4–5 and 6–7 keV points in Figure 3. To look for frequency-dependent change in the feature at $\sim$6 keV, we also produced the same plot for the lowest frequencies ($<2 \times 10^{-5}$). Figure 2 (top) indicates that the lags become larger as we move to lower frequencies, and this is indeed what we see in Figure 4.

The figure shows the lag for both frequency bands $<10^{-4}$ Hz (red continuous line) and $<2 \times 10^{-5}$ Hz (blue dashed line). The lag magnitude increases at lower frequencies. There are even hints of a possible change of shape of the broad line, although not with a high significance. The probability of having different peak energies is $\sim$85% when fitted with Gaussians with different widths.

3.2. Spectral Modeling

To interpret the shape of the lag–energy plot, we turn to spectroscopy. The spectrum of MCG–5-23-16 above 2 keV has been studied extensively. It was established that it has a broad iron line component, but not as extreme as some other objects. Reeves et al. (2007), for example, using *Suzaku* and *XMM* data, measure a line width of 62 eV, and an inner accretion disk radius of 37^{+25}_{-10} r_g when fitted with a diskline model (Fabian et al. 1989). If a full reflection model is used, the inner radius is 26^{+35}_{-8} r_g if the emissivity index is constrained to be $q = 3$ (emissivity $\propto r^{-q}$), and goes to $\sim 6 r_g$ if q is allowed to vary in the fit. Our fit for the *XMM* data gives 90% confidence upper limit on the inner radius of 18 r_g and a best fit of 5.6 r_g and a relatively flat emissivity index $q = 1.8 \pm 0.2$. We used *XMM* spectrum only to remain consistent with the timing analysis.

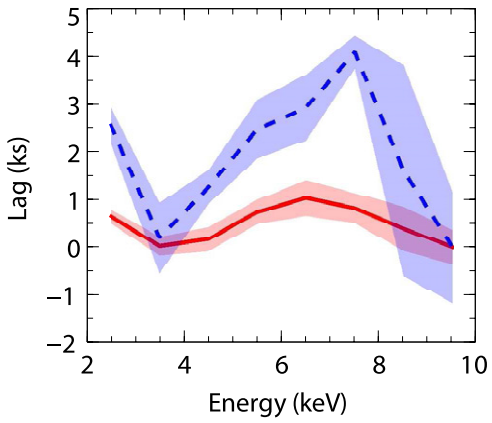

Figure 4. Lag as a function of energy for frequencies $<0^{-4}$ (red; continuous line) and $<2 \times 10^{-5}$ (blue; dashed line) for MCG–5-23-16. The probability that the two lines have different peaks is 85%.

(A color version of this figure is available in the online journal.)

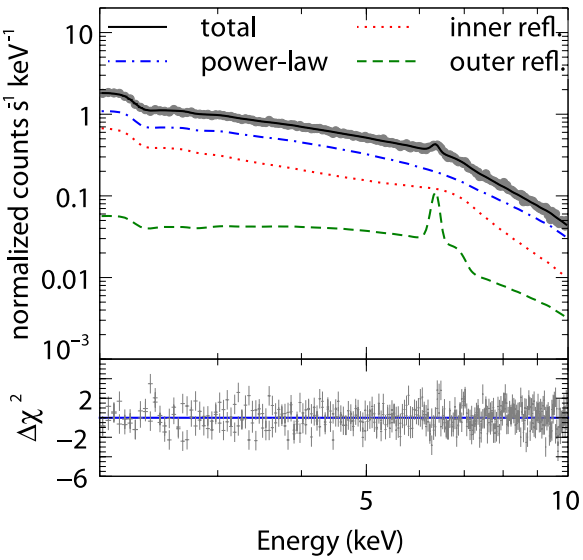

Figure 5. Best-fitting spectral model for MCG–5-23-16. The model includes a power-law component (blue dash-dotted line), outer reflection (green dashed line) modeled with `reflionx`, and a relativistically broadened inner reflection (red dotted line) modeled with `kdblur*reflionx`.

(A color version of this figure is available in the online journal.)

Figure 5 shows the model used to fit the data between 2 and 10 keV, and the best-fitting parameters are presented in Table 1. There are two reflection components modeled using the reflection table `reflionx` (Ross & Fabian 2005): the outer component has a characteristic narrow iron line and originates at large distances from the black hole (molecular torus or broad-line region) and is not expected to produce any variability at the timescale of $\sim$10 ks probed by the lag analysis in Section 3.1. The inner reflection component, modeled with the reflection table `reflionx` broadened by a relativistic kernel `kdblur`, is more likely to be responsible for the lags by responding to variability in the direct power-law component.

Because both power law and reflection contribute to every band between 2 and 10 keV, and if we assume, to a first order,

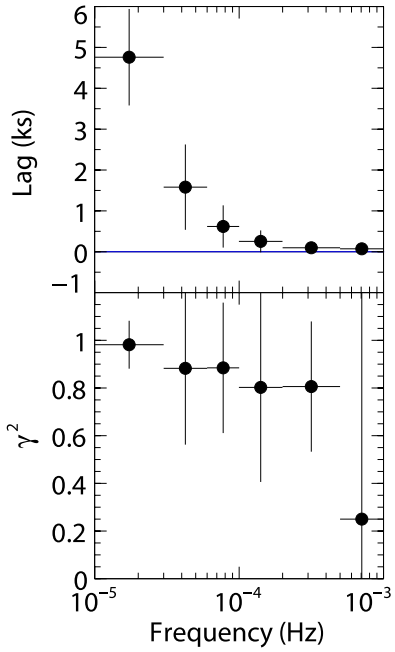

Figure 6. Lag (top) and coherence (bottom) as a function of Fourier frequency between the 4–5 and 6–7 keV energy bands for NGC 7314.

(A color version of this figure is available in the online journal.)

Table 1
Best-fit Parameters

Parameter	MCG–5-23-16	NGC 7314
Absorbing n_h	1.59 ± 0.06	0.44 ± 0.13
Γ	$1.70^{+0.03}_{-0.13}$	1.66 ± 0.05
$r_{\rm in}(r_g)$	$5.6^{+13.1}_{-4.3}$	24^{39}_{15}
Fe abundance (fixed)	1	1
Emissivity index q	2.2 ± 0.5	$2.1^{+0.5}_{-1.4}$
Inclination angle (°)	38^{+9}_{-8}	9^{+10}_{-9}
Gaussian line	...	$6.92^{+0.09}_{-0.06}$ keV
Fe_{broad} equivalent width (eV)	93 ± 13	82^{+19}_{-21}
χ^2/dof	488/381	513/473

the delay between the two components to be energy independent, then each point in the lag plot in Figure 3 gives a measure of the reflection fraction at that energy (variable reflection/power law) multiplied by the intrinsic lag between the power-law and reflection components (see further discussion in Section 5).

4. NGC 7314

4.1. Time Lags

Figure 6 (top) shows the frequency-dependent lags for NGC 7314 between the 4–5 and 6–7 keV bands. Similar to MCG–5-23-16, there is a hard positive lag, where the peak of the iron K line lags the 4–5 keV energy band, with a lag that depends on frequency. Figure 6 (bottom) shows the measured coherence function (see Section 3.1). The two bands have a relatively high coherence of ~0.8 up to $\sim 5 \times 10^{-4}$ Hz.

Similar to the analysis in Section 3.1, we calculate the energy-dependent lags and show them in Figure 7. There is a clear jump in the lag at ~5.5 keV. Its significance is more than 99%. The line profile traced by the lag is narrower than that of MCG–5-23-16 and NGC 4151 (Zoghbi et al. 2012). We also tested for frequency dependence of the profile. The narrow feature at 6–7 keV does not change shape if we select frequencies, say

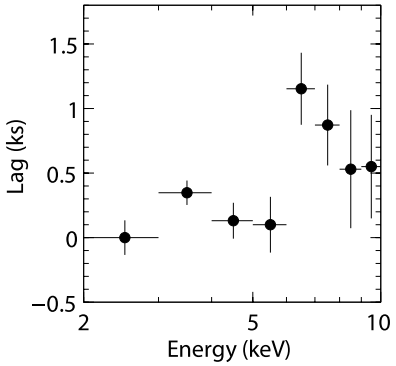

Figure 7. Energy-dependent lag for NGC 7314 at frequency of $(1–30) \times 10^{-5}$ Hz. The whole 2–10 keV band is used as a reference.

$< 5 \times 10^{-5}$ Hz. There is only a change in the magnitude of the lag, which can already be seen in Figure 6 (top). The constant shape with frequency is probably due to the sharpness of the jump (or equivalently, the narrowness of the line), making it difficult to detect a shape change.

4.2. Spectral Modeling

We also performed spectral fitting of the *XMM* observations. Previous spectral decomposition based on variability showed that the spectrum at ~6 keV contains a narrow peak and wing (Yaqoob et al. 1996), indicating that it possibly contains a broad component. Using the high-resolution capabilities of *Chandra*, Yaqoob et al. (2003) showed that the spectrum also contains emission from ions up to Fe XVII at ~6.4 keV, as well as transient emission features from high ionization species Fe XXV and Fe XXVI Lyα. All these lines appear to be variable and respond to continuum changes in less than 12 ks. Although it would be interesting to attribute the lags in Figure 7 to a particular line or ionization state, the energy resolution of the lags permitted by the current data (without significantly affecting the signal) cannot achieve that and remains to be explored with future data.

The spectrum from the *XMM* observation was analyzed. There is a clear line at ~6.4 keV. If fitted with a Gaussian, it has an energy of 6.43 ± 0.02 keV and a width of 126 ± 35 eV, slightly resolved. To model it properly, we included the partially ionized reflection table model `reflionx` in addition to an absorbed power law. The residuals show the presence of a line at ~6.9 keV, which was modeled using a narrow Gaussian. This could be due to Fe XXVI (see Ebrero et al. 2011 for full spectrum analysis). There were also residuals at the wings of the 6.4 keV line that are not accounted for by the cold reflection model. This could be due to a broad component (Yaqoob et al. 1996) and we model them with a Gaussian or a broad relativistic line `laor` (Laor 1991).

Although the broad component is not very broad, its presence is very significant (>99.999% confidence when fitted with a Gaussian). The inner radius of the emitting region from the `laor` model is not very constrained, but it extends down to 13 r_g with an optimum value of 24 r_g, with nearly face-on viewing angle of $\theta = 9°$ and a flat emissivity of $q = 2$, similar to the results found by Yaqoob et al. (2003) using *Chandra* observations and different arguments. The best-fitting model is shown in Figure 8, and the best-fitting parameters are presented in Table 1. It should be noted that, although these are the optimum parameters, their uncertainties are relatively large. If more sophisticated models are used (e.g., `kdblur*reflionx`), we obtain parameters that are similar to those obtained from using the `laor` model.

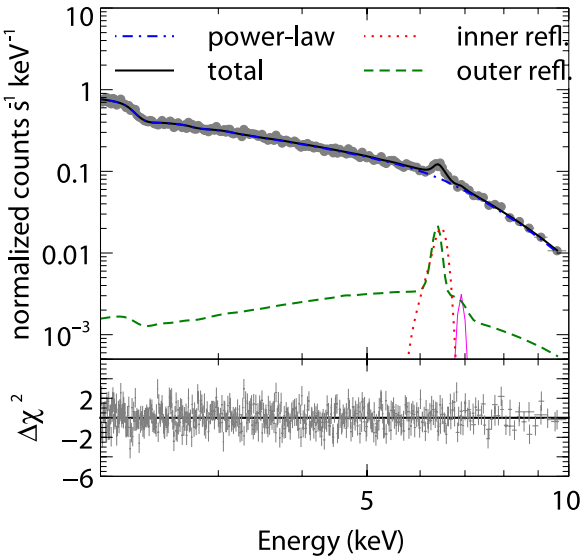

Figure 8. Best-fitting spectral model for NGC 7314. The model includes a power-law component (blue dash-dotted line), outer reflection (green dashed line) modeled with `reflionx` (setting the ionization parameter to the lowest possible value of 1), and an inner reflection (red dotted line), modeled with `laor` and a narrow Fe XXVI line.

(A color version of this figure is available in the online journal.)

Although it is not our aim to do detailed spectral modeling, it is very clear that the spectroscopy is very consistent with lag measurements made in Section 4.1 (Figure 7), where there is a narrow line-like feature in the lag–energy plot. As we discussed in Section 3.1, the lag–energy plot, under simple assumptions, gives a measure of the reflection fraction as a function of energy (the variable reflection component responding to the direct power-law variations), and a reflection fraction that has a line peaking at ∼6.4 keV is very consistent with the spectral modeling.

5. DISCUSSION

We have reported on the discovery of X-ray reverberation in two bright AGN in the iron *K* band. The analysis in Sections 3.1 and 4.1 presents *model-independent* measurements of time lags between the 6–7 keV band, where the Fe Kα line peaks, and other bands, in the sense that this band always lags bands above and below. It is very apparent that these lags are linked to the emission in the Fe Kα band and are very likely due to a reflection process.

The measurement of lag as a function of energy provides a way of measuring the reflection fraction as a function of energy in a completely independent way from the standard spectrum. This provides an invaluable tool to break the degeneracy often encountered in spectroscopic modeling, where it is often difficult to identify an underlying continuum due to absorption and emission complexities. To see how the lag–energy plot measures the reflection fraction, consider the following (see Poutanen 2001; Kotov et al. 2001): let $S_{\rm d}(E,t)$ and $S_{\rm ref}(E,t)$ be the direct and reflected time-dependent spectra, respectively, so that the total observed spectrum is

$$S(E,t) = S_{\rm d}(E,t) + S_{\rm ref}(E,t). \quad (1)$$

Assuming that the direct component changes only in intensity and not in shape, we can write

$$S_{\rm d}(E,t) = D(E)A(t), \quad (2)$$

and the reflection can then be written as

$$S_{\rm ref}(E,t) = f R(E) \int A(t-\tau)T(\tau)d\tau, \quad (3)$$

where $D(E)$ and $R(E)$ are the direct and reflected spectra, respectively, $A(t)$ is the normalization of the direct component, $T(\tau)$ is the transfer function of the reflected component, and f is a constant that contains information about the geometry of the system. We have assumed again that $R(E)$ only changes in amplitude as it varies. The frequency-resolved phase lag as a function of energy is then:

$$\tan(\phi(E,f)) = \frac{\mathrm{Im}[\hat{S}^*(E,f)\hat{D}(E,f)]}{\mathrm{Re}[\hat{S}^*(E,f)\hat{D}(E,f)]}, \quad (4)$$

where $\hat{}$ denotes the Fourier transform and $*$ denotes the complex conjugate. Re and Im indicate the real and imaginary parts of a complex quantity, respectively. This, for small reflection fractions, then reduces to

$$\tan(\phi(E,f)) = f\frac{R(E)}{D(E)}\mathrm{Im}[\hat{T}(f)]. \quad (5)$$

Therefore, for a single frequency band, the lag as a function of energy (e.g., Figures 4 and 7) gives a measure of the reflection fraction as a function of energy.

Could these lags be due to the narrow Fe Kα component? Narrow Fe Kα lines are very common in AGN spectra. Although their origin is still not very clear (molecular torus, the broad-line region, or the outer parts of the disk itself; e.g., Nandra 2006), it is known that the narrow component of the line is not very variable generally, and certainly not on the timescales probed by a typical single observation (∼100 ks) such as those presented here (e.g., Vaughan & Fabian 2004; Bhayani & Nandra 2010). For the data used in this work, we calculated the rms spectra to assess the level of variability as a function of energy. We found that there is a drop in the rms at ∼6 keV. The width of the trough cannot, however, be constrained by the data, and cannot therefore be used to confirm or rule out the origin of variability in the narrow component.

There are, however, other lines of evidence against the observed lags being due to the narrow Fe Kα line. The lags presented here, and that of NGC 4151 (Zoghbi et al. 2012), appear in energy dependence to be a continuation of the lags seen in the soft excess in many NLS1 galaxies. This is particularly apparent in the lag–energy dependence of 1H0707−495 (Zoghbi et al. 2011; Kara et al. 2013a), RE J1034+396 (Zoghbi & Fabian 2011), and IRAS 13224 (Kara et al.). Also, as in the case of NGC 4151, the observed peak in the lag–energy spectrum is less than 6.4 keV. If it were produced by the narrow component, the peak would be at the rest-frame energy of the Fe line. Furthermore, the fact that the lag–energy shape depends on timescale (i.e., temporal frequency) argues again against an origin in the narrow component.

Now we consider the magnitude of the lags. The light-crossing time around a black hole at a radius r (in units of $r_g = GM/c^2$) is $5M_6 r$ s, where M_6 is the black hole mass in units of $10^6\ M_\odot$. For $M_6 = [50, 5]$, where the first number is for MCG–5-23-16 and the second for NGC 7314, the measured inner radii of emission inferred from the spectral fitting of $r = [5.6, 24]$ (in r_g) give a light-crossing time of $[1.4, 0.6]$ ks, within a factor of two of the measured delays in Figures 3 and 7. It should be noted, however, that associating the measured

lag directly with a particular radius is not straightforward. There are many factors that need to be considered. First, the measured lags in Figures 4 and 7 include a dilution factor (Equation (5)) that includes the reflection fraction which makes the measured lags between bands *smaller* than the intrinsic lags between the direct and reflected components. On the other hand, the effects of geometry and gravitational Shapiro delays make the radii inferred from light-crossing estimates *larger* than they are. For example, if the illuminating source is high above the disk, which could be the case for NGC 7314, then the delay is larger than the light-crossing time at the radius of emission inferred from spectral fitting. Accounting for these effects requires full modeling that is beyond the scope of this work (see, e.g., Wilkins & Fabian 2013) and would require more data to study the lag–energy in finer energy bins and frequency bands.

Furthermore, as Figures 2 and 6 show, the lag is frequency dependent and a single measured lag at a single frequency cannot be trivially linked to a particular radius. It is, however, tempting to broadly associate small lags at small timescales with small radii and longer lags with larger radii. The reason is that the competing effects of dilution versus geometry and gravitational delays roughly cancel out (though not exactly; see Wilkins & Fabian 2013). Therefore, the increase in the lag magnitude seen in Figure 4 with decreasing Fourier frequency is likely caused by small timescale variations at small radii (and hence small lags) being filtered out. The effect is similar to, and strongly supported by, the timescale-dependent shape of the lag–energy spectrum of NGC 4151 (Zoghbi et al. 2012). This highlights the power of these plots that measure the reflection fraction independently of the classical spectrum, allowing us to use our knowledge of how the reflection fraction changes with timescales to interpret the lags and the spectra.

It is also interesting to examine the timescale axis of the variability (i.e., Fourier frequency axis). Although the variability in black holes is well established by observations, it is not clear what physical timescale in the accretion disk it represents. For example, if we consider the viscous timescales $t_v = 5r^{1.5}\alpha^{-1}(H/R)^{-2}M_6$ s, where r and M_6 are again in units of r_g and 10^6 $M_\odot$, respectively, and α is the disk viscosity parameter (Frank et al. 2002), then the measured radii from the spectral fitting of [5.6, 24] r_g give a viscous frequency $1/t_v$ of $[7 \times 10^{-8}, 8 \times 10^{-8}]$ Hz, using $\alpha = 0.1$ and $(H/R) = 0.05$. The measured lags clearly span higher frequencies (shorter timescales) than this. If instead thermal timescales are considered, where $t_{\rm th} = (H/R)^2 t_v$, then the measured radii give frequencies of $\sim 3 \times 10^{-5}$ Hz in both cases, which fall exactly in the observed range over which the reverberation lag is measured. Thermal timescales could dominate if variability in density and/or ionization is important. Thermal timescale also seems to be most relevant in the case of accreting white dwarfs too (e.g., Scaringi et al. 2013 for some recent results).

In summary, we have presented lag measurements in the Fe K band that show the peak of the line 6–7 keV band lagging bands either side of it. These simple measurements are model independent, and to interpret them, we showed that they are consistent with a broad iron line responding to variations in an illuminating continuum. Most of the emission originates at 5 r_g for MCG–5-23-16 and 24 r_g for NGC 7314. These two objects are selected for their brightness and high variability, two other variable NLS1 appear to show similar iron K lags (Kara et al. 2013a, 2013b), which is a possible indication that these lags are common among variable objects. The question of how common are they among radio-quiet AGN in general remains, however, to be explored.

REFERENCES

Bhayani, S., & Nandra, K. 2010, MNRAS, 408, 1020
Braito, V., Reeves, J. N., Dewangan, G., et al. 2006, AN, 327, 1067
Cackett, E. M., Fabian, A. C., Zoghbi, A., et al. 2013, ApJ, 764, 9
Chartas, G., Kochanek, C. S., Dai, X., et al. 2012, ApJ, 757, 137
De Marco, B., Ponti, G., Cappi, M., et al. 2013, MNRAS, 339
de Marco, B., Ponti, G., Uttley, P., et al. 2011, MNRAS, 417, L98
Dewangan, G. C., & Griffiths, R. E. 2005, ApJL, 625, L31
Ebrero, J., Costantini, E., Kaastra, J. S., de Marco, B., & Dadina, M. 2011, A&A, 535, A62
Emmanoulopoulos, D., McHardy, I. M., & Papadakis, I. E. 2011, MNRAS, 416, L94
Fabian, A. C., Kara, E., Walton, D. J., et al. 2012a, MNRAS, 419, 116
Fabian, A. C., Rees, M. J., Stella, L., & White, N. E. 1989, MNRAS, 238, 729
Fabian, A. C., Zoghbi, A., Ross, R. R., et al. 2009, Natur, 459, 540
Fabian, A. C., Zoghbi, A., Wilkins, D., et al. 2012b, MNRAS, 419, 116
Frank, J., King, A., & Raine, D. J. 2002, Accretion Power in Astrophysics (3rd ed.; Cambridge: Cambridge Univ. Press)
Guilbert, P. W., & Rees, M. J. 1988, MNRAS, 233, 475
Haardt, F., & Maraschi, L. 1991, ApJL, 380, L51
Kara, E., Fabian, A. C., Cackett, E. M., et al. 2013a, MNRAS, 428, 2795
Kara, E., Fabian, A. C., Cackett, E. M., Miniutti, G., & Uttley, P. 2013b, MNRAS, 428, 2795
Kotov, O., Churazov, E., & Gilfanov, M. 2001, MNRAS, 327, 799
Laor, A. 1991, ApJ, 376, 90
Mattson, B. J., & Weaver, K. A. 2004, ApJ, 601, 771
Miller, J. M. 2007, ARA&A, 45, 441
Miller, L., Turner, T. J., Reeves, J. N., & Braito, V. 2010, MNRAS, 408, 1928
Nandra, K. 2006, MNRAS, 368, L62
Nandra, K., Barret, D., Fabian, A., et al. 2012, ExA, 34, 445
Nowak, M. A., Vaughan, B. A., Wilms, J., Dove, J. B., & Begelman, M. C. 1999, ApJ, 510, 874
Poutanen, J. 2001, AdSpR, 28, 267
Reeves, J. N., Awaki, H., Dewangan, G. C., et al. 2007, PASJ, 59, 301
Reynolds, C. S., & Nowak, M. A. 2003, PhR, 377, 389
Reynolds, C. S., Young, A. J., Begelman, M. C., & Fabian, A. C. 1999, ApJ, 514, 164
Risaliti, G., Elvis, M., Fabbiano, G., et al. 2007, ApJL, 659, L111
Ross, R. R., & Fabian, A. C. 1993, MNRAS, 261, 74
Ross, R. R., & Fabian, A. C. 2005, MNRAS, 358, 211
Scaringi, S., Koerding, E., Uttley, P., et al. 2013, MNRAS, 347
Schulz, H., Knake, A., & Schmidt-Kaler, T. 1994, A&A, 288, 425
Tanaka, Y., Nandra, K., Fabian, A. C., et al. 1995, Natur, 375, 659
Vaughan, B. A., & Nowak, M. A. 1997, ApJL, 474, L43
Vaughan, S., & Fabian, A. C. 2004, MNRAS, 348, 1415
Vaughan, S., Uttley, P., Pounds, K. A., Nandra, K., & Strohmayer, T. E. 2011, MNRAS, 413, 2489
Wandel, A., & Mushotzky, R. F. 1986, ApJL, 306, L61
Weaver, K. A., Yaqoob, T., Mushotzky, R. F., et al. 1997, ApJ, 474, 675
Wilkins, D. R., & Fabian, A. C. 2013, MNRAS, 428, 2795
Yaqoob, T., George, I. M., Kallman, T. R., et al. 2003, ApJ, 596, 85
Yaqoob, T., Serlemitsos, P. J., Turner, T. J., George, I. M., & Nandra, K. 1996, ApJL, 470, L27
Zoghbi, A., & Fabian, A. C. 2011, MNRAS, 418, 2642
Zoghbi, A., Fabian, A. C., Reynolds, C. S., & Cackett, E. M. 2012, MNRAS, 422, 129
Zoghbi, A., Fabian, A. C., Uttley, P., et al. 2010, MNRAS, 401, 2419
Zoghbi, A., Uttley, P., & Fabian, A. C. 2011, MNRAS, 412, 59